AIAA 82-4200

Influence of Unsteady Aerodynamics on Hingeless Rotor Ground Resonance

Wayne Johnson*
NASA Ames Research Center, Moffett Field, Calif.

Calculations of the modal frequency and damping for a hingeless rotor on a gimballed support in hover are compared with measured results for two configurations (differing in blade flap stiffness). Good correlation is obtained when an inflow dynamics model is used to account for the influence of the unsteady aerodynamics. The effect of the unsteady aerodynamics is significant for this rotor system. The inflow dynamics model introduces additional states corresponding to perturbations of the wake-induced velocity at the rotor disk. The calculations confirm the experimental observation that the inflow mode introduced by these additional states is measurable for one configuration but not for the other.

Nomenclature

C = lift deficiency function
M = body pitch moment
s = eigenvalue, $=\sigma \pm i\omega$
β_P = progressing (high-frequency) flap mode
β_R = regressing (low-frequency) flap mode
ζ = damping ratio, $-\mathrm{Re}s/|s|$
ζ_P = progressing (high-frequency) lag mode
ζ_R = regressing (low-frequency) lag mode
θ = body pitch mode; body pitch degree of freedom
κ = factor in time lag of inflow
λ = inflow mode
λ_0 = inflow ratio: mean induced velocity of rotor divided by tip speed
λ_x = longitudinal induced velocity perturbation
λ_y = lateral induced velocity perturbation
σ = modal damping, $=\mathrm{Re}s$
ϕ = body roll mode; body roll degree of freedom
ω = modal frequency, $=\mathrm{Im}s$; system excitation frequency
Ω = rotor rotational speed

Introduction

THE importance of unsteady aerodynamic forces in aeroelastic phenomena has long been acknowledged, based on both fixed wing and rotary wing experience. Yet an entirely satisfactory model for the unsteady aerodynamics of a helicopter rotor is still not available, particularly for problems such as flutter stability and handling qualities that involve transient motion of the system. A model for the noncirculatory loads can be readily obtained from two-dimensional unsteady airfoil theory, but the results from either two-dimensional or fixed-wing three-dimensional wing theory for the circulatory loads are not applicable since the wake models are not correct for rotary wings. The development of a general theory for rotary wing unsteady airloads is difficult owing to the complex geometry of the rotor wake, even in hover. Moreover, in forward flight a time-invariant model of the system is not possible owing to the periodically varying aerodynamic environment of the blades. Consequently, attention has recently been focused on the development of relatively simple models for the unsteady aerodynamics. These models take the form of differential equations for parameters defining the wake-induced velocity distribution at the rotor disk.

The development of such an inflow dynamics model involves two steps. The first step is the identification, from analysis or experiment, of the structure and parameters of the unsteady aerodynamics model. The second step is the verification of the model by correlation of calculations and measurements for progressively more diverse and complex aeroelastic problems. Considerable progress has been made with the first step, although much remains to be done. The present paper is a contribution to the second step. Bousman[1] has produced a set of experimental data that provides an opportunity to examine the influence of inflow dynamics on the coupled behavior of a rotor and body. In the sections below, the inflow dynamics model used and the experimental system will be described. Then the measured data will be compared to calculations obtained with and without the inflow dynamics model, and the influence of unsteady aerodynamics on this system will be discussed.

Perturbation Inflow Model for Rotor Unsteady Aerodynamics

The inflow dynamics model used here is derived in detail in Refs. 2 and 3. For the present purposes, only the inflow perturbation due to pitch and roll moments in hover is considered. A wake-induced velocity perturbation that varies linearly over the rotor disk is defined by

$$\delta\lambda = \lambda_x r\cos\psi + \lambda_y r\sin\psi$$

where r and ψ are the polar coordinates of the disk. The variables λ_x and λ_y are related to the aerodynamic pitch and roll moment coefficients, C_{M_y} and C_{M_x}, by first-order differential equations:

$$\tau\begin{pmatrix}\lambda_x\\ \lambda_y\end{pmatrix}^{\cdot} + \begin{pmatrix}\lambda_x\\ \lambda_y\end{pmatrix} = \frac{\partial\lambda}{\partial M}\begin{pmatrix}-C_{M_y}\\ C_{M_x}\end{pmatrix}_{\text{aero}}$$

where $\tau = \kappa(\partial\lambda/\partial M)$, with κ a constant.

The factor $\partial\lambda/\partial M$ can be obtained from differential momentum theory as follows.[2] A thrust perturbation $\mathrm{d}T$ on the element of disk area $\mathrm{d}A$ is related to the inflow perturbation by $\mathrm{d}T = \dot{m}2\delta v$, where the mass flow rate is $\dot{m} = \rho v_0 \mathrm{d}A$ (v_0 and δv are the mean and perturbation inflow

Received July 1, 1981; revision received Nov. 12, 1981. This paper is declared a work of the U.S. Government and therefore is in the public domain.

*Assistant Chief, Low Speed Aircraft Research Branch. Member AIAA.

velocities, written λ_0 and $\delta\lambda$ when made dimensionless by dividing by the rotor tip speed). Hence

$$\delta v = \frac{dT}{dA}\Big/ 2\rho v_0$$

A linear variation of δv over the rotor disk implies a linear variation of the loading dT/dA, which corresponds to pitch and roll moments. Integration of this expression over the rotor disk then produces $\partial\lambda/\partial M = 2/\lambda_0$. This result for $\partial\lambda/\partial M$ can be derived more rigorously by means of unsteady actuator disk theory.[2,4] Neglecting the time lag, the factor $\partial\lambda/\partial M = 2/\lambda_0$ produces a lift deficiency function of

$$C = \frac{1}{1 + \sigma a/8\lambda_0}$$

(see Ref. 2; here a is the blade section lift curve slope and σ is the rotor solidity ratio), which is identical to the low-frequency approximation to Loewy's lift deficiency function for harmonic loading[5]:

$$C = \frac{1}{1 + \pi/(h/b)}$$

(where h/b is the ratio of the shed wake vertical spacing to the blade semichord, hence $h/b = 4\lambda_0/\sigma$). Dynamic inflow models have also been formulated that use $\partial\lambda/\partial M = 1/\lambda_0$ for the hovering rotor (see, for example, Ref. 6). This smaller value of the factor $\partial\lambda/\partial M$ is obtained by including a variation of the mass flow rate due to the inflow perturbation. The influence of the choice of $\partial\lambda/\partial M$ on the calculations for the present problem is discussed below.

The parameter κ in the inflow time lag is obtained by considering the apparent mass of an impermeable disk subject to an angular acceleration[6]: $\kappa = 16/45\pi = 0.113$. This value is supported by comparison with experimental data[6,7] and by parameter identification results.[8] The value of κ may depend on the rotor mean loading distribution,[9] and there are indications that a larger or smaller value is appropriate in certain cases.[9,10] Without the time lag, $\kappa = 0$, a quasistatic inflow model is obtained, the effects of which are expressed by the lift deficiency function C given above. For rotor dynamics problems in which the dominant aerodynamic forces are the lift perturbations due to angle of attack changes, the magnitude of the aerodynamic influence is described by the blade Lock number (which contains the section lift curve slope). Hence, in such cases, the effects of the quasistatic inflow model can be largely represented by the use of an effective Lock number that is the product of the actual Lock number and the lift deficiency function.[11,12] A quasistatic inflow dynamics model has long been used in handling qualities analyses (see Ref. 13, for example). A very large value of the time lag ($\kappa \to \infty$) would eliminate the influence of the inflow dynamics.

Experimental measurements of hub moment response to cyclic control and shaft oscillations show a significant influence of the inflow dynamics.[6] Calculations of flap-lag stability also predict a significant influence of the inflow dynamics.[14,15] The need for the time lag appears to depend on the problem involved. The influence of the time lag is often enough to be measurable, but the quasistatic model may still give qualitatively correct results. The inflow dynamics model is not quite as well developed for forward flight as for hover, but considerable progress has been made (see Refs. 6, 9, 12, and 14-16).

Description of the Experimental Apparatus

The experimental data considered here were obtained in an investigation of ground resonance stability in hover.[1] A model rotor with hingeless blades, on a gimbal support with pitch and roll degrees of freedom was tested. The primary parameters describing the system are given in Table 1. The experimental apparatus and test techniques are described in detail in Ref. 1. All of the results presented in this paper are for a collective pitch of zero, but the cambered airfoil used has zero lift at an angle of attack of -1.5 deg. Hence the rotor had a small positive thrust value at zero collective pitch. A lift curve slope of 6.59 was used for this airfoil at low Reynolds number. The blades had flap and lag flexures at radial station $0.105R$, with no pitch/flap or pitch/lag couplings. The collective pitch was introduced outboard of the flexures. The blades were very stiff in torsion. Two flap flexures were used: configuration 1, for which the flap flexure had one-fourth the stiffness of the lag flexure; and configuration 4, with equal flap and lag flexure stiffnesses. (The designation "configuration 4" follows Ref. 1.)

The blade lag stiffness was such that the rotating natural frequency of the lag mode was below once-per-revolution for rotor speeds above 445 rpm. The springs on the gimbal produced resonances between the regressing lag mode and the body pitch and roll modes at rotor speeds of about 595 and 765 rpm, respectively. The corresponding natural frequency of the blade lag mode was about 0.80/rev and 0.68/rev for these two resonances. At such resonances, with the blade lag frequency below 1/rev, a ground resonance instability is possible if the system damping is low enough.[2] At the resonance of the regressing lag mode and body roll mode, the blade flap frequency was 1.12/rev for configuration 1, and 1.20/rev for configuration 4.

Description of the Analysis

The aeroelastic stability of this system was calculated using the analysis described in Ref. 3. The only rotor degrees of freedom considered were the fundamental flap and lag modes of each of the three blades. The body degrees of freedom consisted of pitch and roll motion about the gimbal. In hover, the coning and collective lag modes do not couple with such body motion. Hence the analytical model consisted of the rotor cyclic flap, cyclic lag, and body pitch and roll degrees of freedom (12 states). The variables λ_x and λ_y were included when the inflow dynamics model was used (14 states). The parameters required by the analysis were determined from the known values of the geometry, inertias, nonrotating frequencies, and nonrotating damping of the rotor and body.[1]

Results for Configuration 1

In Figs. 1-5 the measured modal frequencies and damping for configuration 1 (the soft flap flexure) as a function of rotor speed are compared with calculations. The collective pitch is zero. The calculated results are for two cases: with and without the inflow dynamics model. The modal frequencies ω

Table 1 Rotor parameters

No. of blades	3
Radius, R	0.811 m
Solidity ratio	0.0494
Lock number	8.4
Twist	0
Tip Mach number (at 1000 rpm)	0.25
Tip Reynolds number (at 1000 rpm)	243,000
Airfoil	NACA 23012
Height hub above gimbal	0.241 m
Nonrotating lag frequency	
Configuration 1	6.70 Hz
Configuration 4	6.73 Hz
Nonrotating flap frequency	
Configuration 1	3.13 Hz
Configuration 4	6.63 Hz

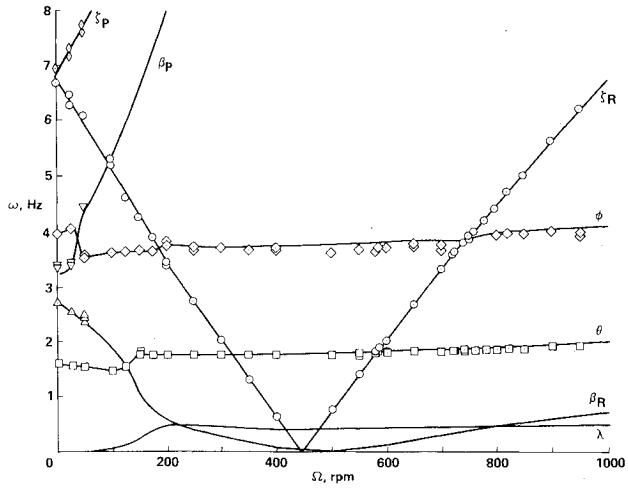

Fig. 1 Modal frequencies as a function of rotor speed for configuration 1: comparison of measurements (points) and calculations including inflow dynamics (lines).

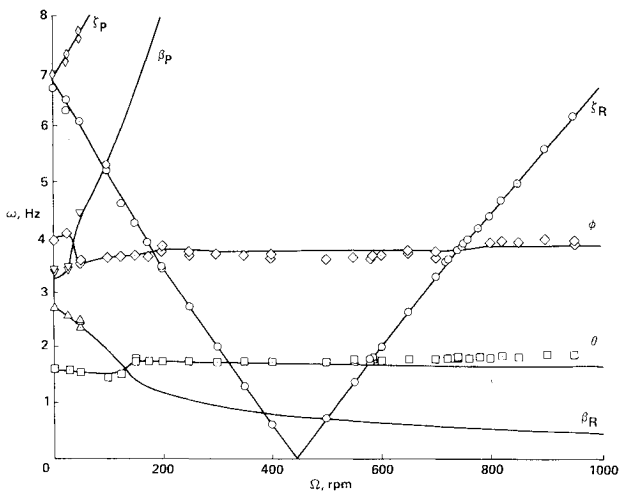

Fig. 2 Modal frequencies as a function of rotor speed for configuration 1: comparison of measurements (points) and calculations without inflow dynamics (lines).

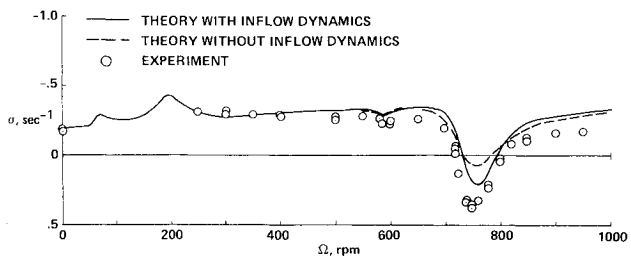

Fig. 3 Regressing lag mode damping as a function of rotor speed for configuration 1.

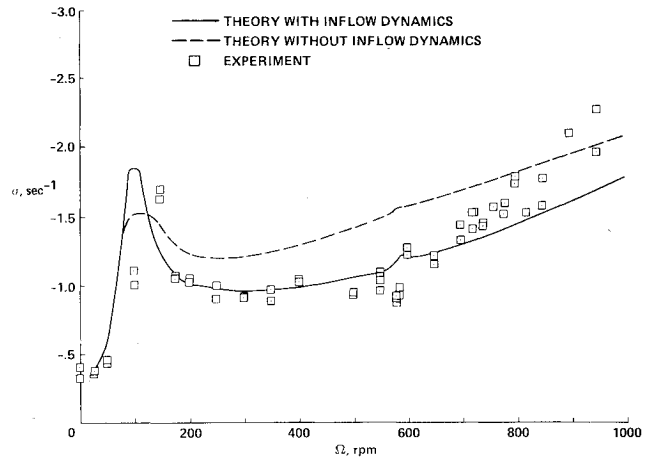

Fig. 4 Body pitch mode damping as a function of rotor speed for configuration 1.

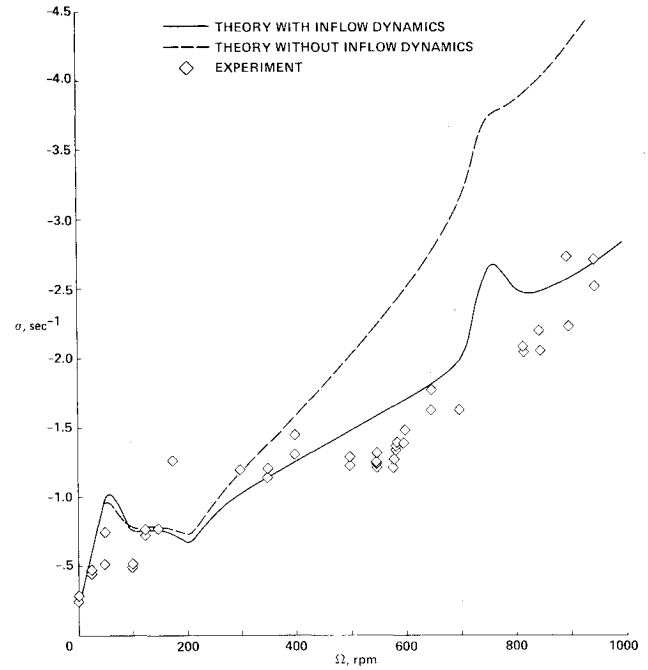

Fig. 5 Body roll mode damping as a function of rotor speed for configuration 1.

are shown in Figs. 1 and 2, and the damping σ of the regressing lag, body pitch, and body roll modes is shown in Figs. 3-5. The eigenvalue is $s = \sigma \pm i\omega$; a mode is unstable if σ is positive. The regressing lag mode damping shows a ground resonance instability due to coupling with the roll mode. The designation of the modes in these and the succeeding figures is defined in the nomenclature list. Without the inflow dynamics model, the calculated frequencies of the body modes are too low for rotor speeds above the resonances (Fig. 2); the lag mode is too stable at the resonance (Fig. 3); the pitch mode damping is too high (Fig. 4); and the roll mode damping is far too high (Fig. 5). The body structural damping is small (note the value at $\Omega = 0$), so the discrepancies in Figs. 4 and 5 are due to the aerodynamic forces. With the inflow dynamics model, the frequencies are predicted well (Fig. 1); the calculation of the lag mode damping is improved, although it is still too stable at the resonance (Fig. 3); the pitch mode damping is predicted well, except that it is somewhat low at high rotor speed (Fig. 4); and the calculated roll mode damping correlates well with the measurements (Fig. 5). The prediction of the lag mode damping at the ground resonance instability could be improved by reducing the structural damping of the rotor lag or body roll motion—if some rational approach for making such a change could be established. Note that there are significant shifts in the body frequencies at low rotor speed due to resonance with the flap modes. Even with the rotor not rotating, the flap and body motions are coupled, with the effect that the flap-pitch and flap-roll frequency pairs move apart. The asymmetry of the body frequencies then produces the split in the regressing and progressing flap frequencies observed at zero rotor speed.

The measured frequencies and regressing lag mode damping were also compared with calculations using the quasistatic inflow model. The nonrotating body frequencies were still predicted well, but the calculated body frequencies were much too high at rotor speeds above about 300 rpm. Consequently the resonances with the lag mode were shifted to higher rotor speeds than in the measurements. In particular the greatest instability at the roll mode resonance was predicted to occur at 800 rpm, instead of 750 rpm as measured. In addition, the body mode damping was not predicted as well as with the complete inflow dynamics model. Hence for this problem the quasistatic inflow model was not acceptable.

Results for Configuration 4

In Figs. 6-11 the measured modal frequencies and damping for configuration 4 (the stiff flap flexure) are compared with calculations. The collective pitch is zero in this case. Without the inflow dynamics model, the correlation is similar to that for configuration 1: the predicted roll mode frequency is too low at rotor speeds above the resonance (Fig. 7); the regressing lag mode is too stable at the roll mode resonance (Fig. 8); and the calculated roll mode damping is much too high (Fig. 9). In addition, the calculated frequency of the pitch mode does not match either of the modes observed below 3 Hz in the experiment (Fig. 7). The calculated regressing flap mode has high damping, and so can not correspond to one of the measured modes. The damping of the pitch mode calculated without the inflow dynamics is shown on both Fig. 10 and Fig. 11, but this comparison is not meaningful since the frequency does not match either measured mode. With the inflow dynamics model, the frequencies are well predicted, except for the roll mode at rotor speeds from 250 to 350 rpm (Fig. 6). As for configuration 1, the prediction of the lag mode damping is improved (Fig. 8); and the correlation of the calculated and measured roll mode damping is very good (Fig. 9). Moreover, now two modes are predicted to occur below 3 Hz, and the calculated modes correlate well with the measured modes in both frequency and damping (Figs. 6, 10, and 11). The low-frequency mode is now identified as the inflow mode, although its eigenvector involves considerable motion of the body and rotor.

For this configuration, the correlation is not good at the resonance between the regressing flap mode and the body roll mode ($\Omega = 250$-350 rpm, Fig. 6). The calculations show much more coupling than the measurements. The same effect is observed in the frequencies calculated without aerodynamic forces (not shown), so the coupling is due to the structural dynamics of the system. This resonance occurs at a flap frequency of about 1.8/rev, which suggests that the problem involves some high-frequency aeroelastic phenomenon. The problem could be a deficiency in the aerodynamic model at high frequencies; or possibly some higher mode of the rotor or body is involved.

The influence of the factor $\partial\lambda/\partial M$ was examined by repeating the frequency and damping calculations using the smaller value discussed above. The effects of using $\partial\lambda/\partial M = 1/\lambda_0$ rather than $\partial\lambda/\partial M = 2/\lambda_0$ were as follows, for both configuration 1 and 4. The only effect on the frequencies was a slight increase in the frequency of the inflow mode at high rotor speed (this frequency is primarily determined by the time lag parameter κ). The effects on the frequencies of the lag and body modes were negligible. There was also no effect on the calculated lag mode damping. The calculated body damping was slightly higher for rotor speeds above 800 rpm, so the correlation with experiment became somewhat better for the pitch mode but was not as good for the roll mode. The only significant influence of $\partial\lambda/\partial M$ was on the inflow mode damping. At high rotor speeds the inflow mode damping calculated was 75-80% larger for configuration 1, and 50-70% larger for configuration 4. For configuration 4, the inflow mode damping calculated using $\partial\lambda/\partial M = 1/\lambda_0$ was approximately $\sigma = -3$ for $\Omega > 650$ rpm. This is 45-50% higher than the measured values. Using $\partial\lambda/\partial M = 2/\lambda_0$, at these rotor speeds $-\sigma < 2$ is obtained, which is 5-10% lower than the measurements (see Fig. 11). Hence, in general, the influence of $\partial\lambda/\partial M$ on the calculated dynamics is small for this problem, although $\partial\lambda/\partial M = 2/\lambda_0$ did produce better correlation with the measured inflow mode damping for configuration 4. This low sensitivity to the parameters is necessary if effective use is to be made of such a simple theoretical model for rotor unsteady aerodynamics.

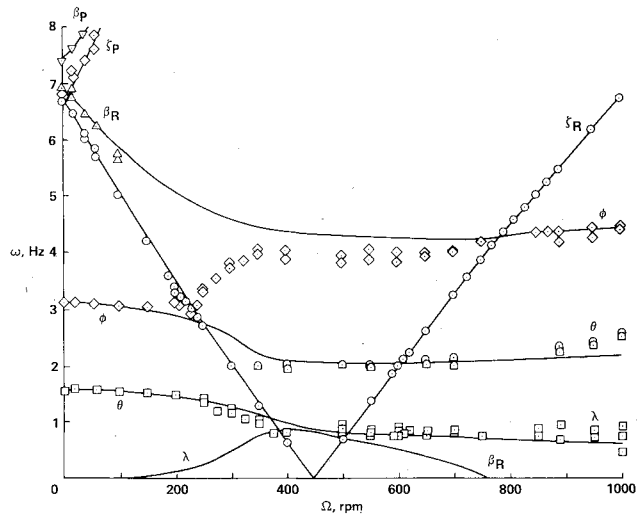

Fig. 6 Modal frequencies as a function of rotor speed for configuration 4: comparison of measurements (points) and calculations including inflow dynamics (lines).

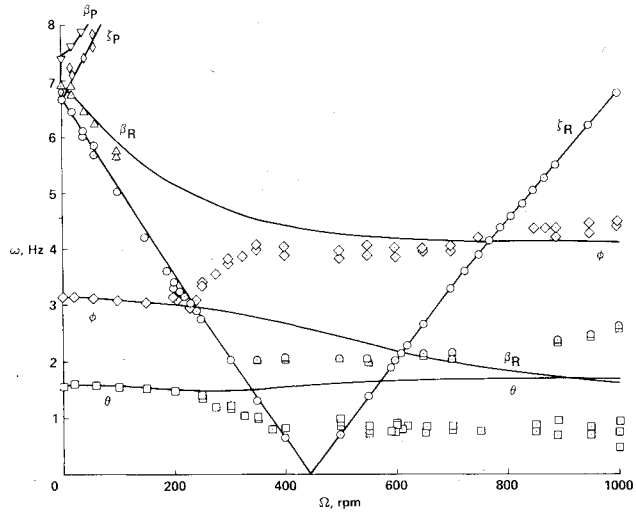

Fig. 7 Modal frequencies as a function of rotor speed for configuration 4: comparison of measurements (points) and calculations without inflow dynamics (lines).

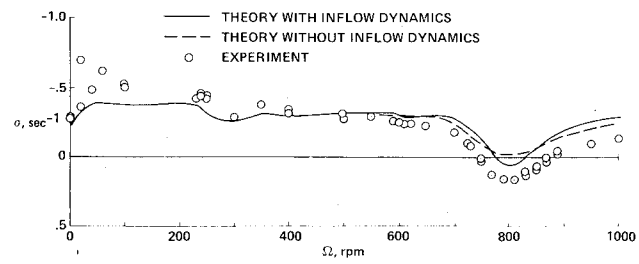

Fig. 8 Regressing lag mode damping as a function of rotor speed for configuration 4.

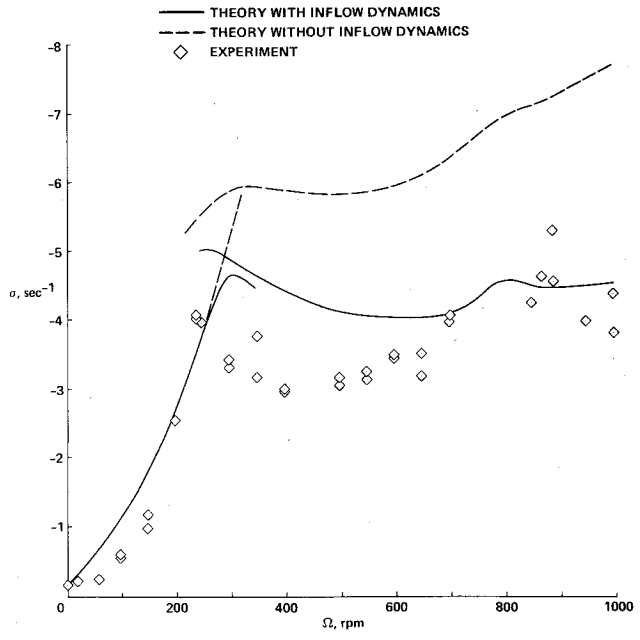

Fig. 9 Body roll mode damping as a function of rotor speed for configuration 4.

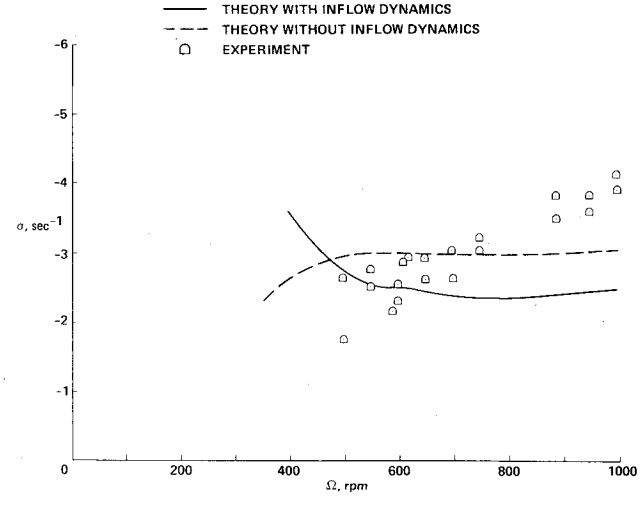

Fig. 10 Body pitch mode damping as a function of rotor speed for configuration 4.

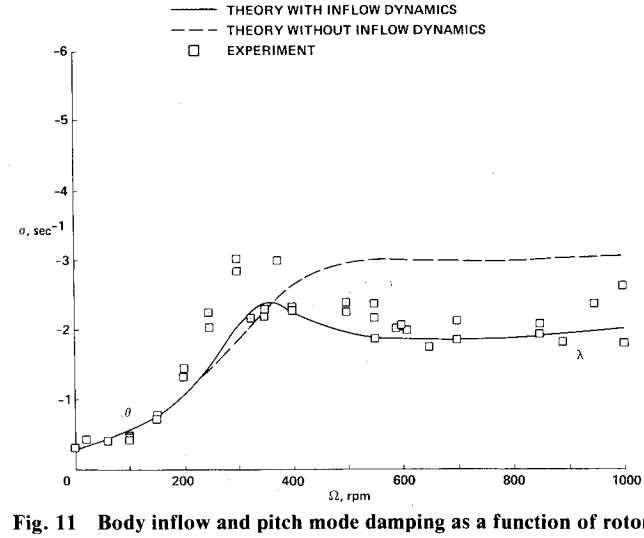

Fig. 11 Body inflow and pitch mode damping as a function of rotor speed for configuration 4.

Table 2 Body pitch and inflow mode characteristics (Ω = 650 rpm)

	Configuration 1	Configuration 4
Pitch mode		
Frequency, Hz	1.84	2.08
Damping ratio	0.11	0.19
Inflow mode		
Frequency, Hz	0.43	0.74
Damping ratio	0.59	0.37
Ratio contributions of inflow and pitch modes to pitch motion	0.08	0.30

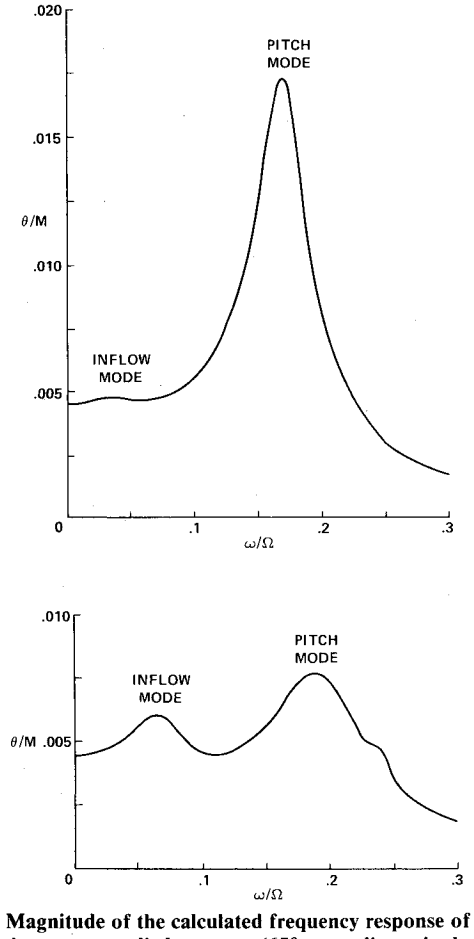

Fig. 12 Magnitude of the calculated frequency response of the body pitch motion to an applied moment (650 rpm; dimensionless scales); a) Configuration 1, b) Configuration 4.

The successful prediction of the low-frequency modes measured in the test of configuration 4 raises further questions. First, what is this inflow mode? That it is measurable is surprising, since in fact the inflow variables λ_x and λ_y do not correspond to real physical states of the system. This mode may be interpreted as follows. The unsteady aerodynamics introduces behavior of the system, as observed in either the time or frequency domain, that can be approximated by an additional oscillatory mode with low or moderate damping (the experimental procedure used to measure the frequency and damping only works for such modes). Approximating the behavior by an additional mode implies then the existence of additional states or degrees of freedom of the system.

The second question is why the inflow mode was observed in the tests of configuration 4, but not for configuration 1?

With increased flap stiffness, the regressing flap mode will be more coupled with the body motion. The great coupling between the flap motion and inflow variables then implies that the inflow dynamics will have more influence on the body motions for configuration 4 than for configuration 1. The pitch and inflow modes were measured by applying a pitch moment impulse to the body. Then the modal frequencies were identified from the magnitude of the spectrum of the resulting transient pitch motion; and the corresponding damping was estimated using the moving block technique.[1] Consider what the calculations imply about the task of identifying the pitch and inflow modes from the body motion. Table 2 summarizes the characteristics of the low-frequency modes for the two configurations. For configuration 4 relative to configuration 1, the damping ratio of the pitch mode is increased while the damping ratio of the inflow mode is decreased. This implies that the inflow mode will be more observable for configuration 4, since the damping ratio determines the relative width of the resonant peaks. Note that with a damping ratio of 0.6, the frequency response will hardly show a resonant peak at all. In addition, the small frequency of the inflow mode for configuration 1 would make it more difficult to measure that mode, since the experimental data reduction procedure had a frequency resolution of 0.2 Hz. The modal contribution can be quantified by considering the ratio of the coefficients of the pitch and inflow modes in the partial fraction expansion of the pitch response. This ratio is 8% for configuration 1, and 30% for configuration 4 (Table 2; the next largest contributions, from the regressing flap and lag modes, are approximately 10% of the contribution of the inflow mode). The frequency response of the body pitch motion to an applied moment is shown in Fig. 12 for the two configurations. The calculations confirm that the inflow mode should be observable for configuration 4, but not for configuration 1.

Conclusions

Calculations of the modal frequencies and damping for a hingeless rotor on a gimballed support in hover have shown good correlation with measurements when an inflow dynamics model is used to account for the influence of unsteady aerodynamics. The influence of the unsteady aerodynamics was significant for this system. One of the modes in the measured data has been identified as an inflow mode, demonstrating that the unsteady aerodynamics are well represented by an augmented state model in this case, and that the inflow dynamics mode is directly measurable. The sensitivity of the calculations to the choice of the parameter $\partial\lambda/\partial M$ in the inflow model was found to be small for this problem. The remaining discrepancy between the measured and calculated results involved the resonance between the flap and roll modes at low rotor speed for configuration 4. Further development and verification of this inflow dynamics model will require comparison with data for additional rotor systems, and extension of these investigations to forward flight.

References

[1] Bousman, W.G., "An Experimental Investigation of the Effects of Aeroelastic Couplings on Aeromechanical Stability of a Hingeless Rotor Helicopter," *Journal of the American Helicopter Society,* Vol. 26, No. 1, Jan. 1981, pp. 46-54.

[2] Johnson, W., *Helicopter Theory,* Princeton University Press, Princeton, New Jersey, 1980.

[3] Johnson, W., "A Comprehensive Analytical Model of Rotorcraft Aerodynamics and Dynamics," NASA TM 81182, June 1980.

[4] Miller, R.H., "Rotor Blade Harmonic Air Loading," *AIAA Journal,* Vol. 2, July 1964, pp. 1254-1269.

[5] Loewy, R.G., "A Two-Dimensional Approximation to the Unsteady Aerodynamics of Rotary Wings," *Journal of the Aeronautical Sciences,* Vol. 24, Feb. 1957, pp. 81-92.

[6] Peters, D.A., "Hingeless Rotor Frequency Response with Unsteady Inflow," NASA SP-352, Feb. 1974.

[7] Carpenter, P.J. and Fridovich, B., "Effect of a Rapid Blade-Pitch Increase on the Thrust and Induced-Velocity Response of a Full-Scale Helicopter Rotor," NACA TN 3044, Nov. 1953.

[8] Banerjee, D., Crews, S.T., Hohenemser, K.H., and Yin, S.K., "Identification of State Variables and Dynamic Inflow from Rotor Model Dynamic Tests," *Journal of the American Helicopter Society,* Vol. 22, No. 2, April 1977, pp. 28-36.

[9] Pitt, D.M. and Peters, D.A., "Theoretical Prediction of Dynamic Inflow Derivatives," *Vertica,* Vol. 5, No. 1, 1981, pp. 21-34.

[10] Rebont, J., Valensi, J., and Soulez-Lariviere, J., "Response of a Helicopter Rotor to an Increase in Collective Pitch for the Case of Vertical Flight," NASA TT F-55, Jan. 1961.

[11] Curtiss, H.C. Jr. and Shupe, N.K., "A Stability and Control Theory for Hingeless Rotors," Annual National Forum of the American Helicopter Society, Washington, D.C., May 1971.

[12] Ormiston, R.A. and Peters, D.A., "Hingeless Helicopter Rotor Response with Nonuniform Inflow and Elastic Blade Bending," *Journal of Aircraft,* Vol. 9, Oct. 1972, pp. 730-736.

[13] Seckel, E., *Stability and Control of Airplanes and Helicopters,* Academic Press, New York, 1964.

[14] Gaonkar, G.H. and Peters, D.A., "Use of Multiblade Coordinates for Helicopter Flap-Lag Stability with Dynamic Inflow," *Journal of Aircraft,* Vol. 17, Feb. 1980, pp. 112-118.

[15] Peters, D.A. and Gaonkar, G.H., "Theoretical Flap-Lag Damping with Various Dynamic Inflow Models," *Journal of the American Helicopter Society,* Vol. 25, No. 3, July 1980, pp. 29-36.

[16] Banerjee, D., Crews, S.T., and Hohenemser, K.H., "Parameter Identification Applied to Analytic Hingeless Rotor Modelling," *Journal of the American Helicopter Society,* Vol. 24, No. 1, Jan. 1979, pp. 26-32.